Geometrically unrestricted, topologically constrained control of liquid crystal defects using simultaneous holonomic magnetic and holographic optical manipulation

Michael C. M. Varney,[1] Nathan J. Jenness,[2] and Ivan I. Smalyukh[1,3,4,*]

[1]*Department of Physics, University of Colorado at Boulder, Boulder, Colorado 80309, USA*

[2]*Department of Mechanical Engineering, University of Rochester, Rochester, New York 14627, USA*

[3]*Department of Electrical, Computer, and Energy Engineering, Materials Science and Engineering Program, Liquid Crystals Materials Research Center, University of Colorado at Boulder, Boulder, Colorado 80309, USA*

[4]*Renewable and Sustainable Energy Institute, National Renewable Energy Laboratory and University of Colorado at Boulder, Boulder, Colorado 80309, USA*

(Received 16 December 2013; published 13 February 2014)

Despite the recent progress in physical control and manipulation of various condensed matter, atomic, and particle systems, including individual atoms and photons, our ability to control topological defects remains limited. Recently, controlled generation, spatial translation, and stretching of topological point and line defects have been achieved using laser tweezers and liquid crystals as model defect-hosting systems. However, many modes of manipulation remain hindered by limitations inherent to optical trapping. To overcome some of these limitations, we integrate holographic optical tweezers with a magnetic manipulation system, which enables fully holonomic manipulation of defects by means of optically and magnetically controllable colloids used as "handles" to transfer forces and torques to various liquid crystal defects. These colloidal handles are magnetically rotated around determined axes and are optically translated along three-dimensional pathways while mechanically attached to defects, which, combined with inducing spatially localized nematic-isotropic phase transitions, allow for geometrically unrestricted control of defects, including previously unrealized modes of noncontact manipulation, such as the twisting of disclination clusters. These manipulation capabilities may allow for probing topological constraints and the nature of defects in unprecedented ways, providing the foundation for a tabletop laboratory to expand our understanding of the role defects play in fields ranging from subatomic particle physics to early-universe cosmology.

DOI: 10.1103/PhysRevE.89.022505 PACS number(s): 61.30.Jf

I. INTRODUCTION

Topological defects play important roles in many branches of physics, ranging from early-universe cosmology [1,2] and string theory [3,4] to condensed matter physics [5]. Although theoretical studies of topological defects have progressed in many fields, their experimental exploration remains difficult in noncondensed matter systems, such as cosmology, where researchers deal with probing observable consequences of these defects on cosmic scales. For instance, analysis of NASA's Cosmic Background Explorer satellite data provides insights into possible cosmic string imprints on the large-scale structure of the Universe [6]. Tabletop physics, on the other hand, provides an opportunity to study phenomena of particle physics and cosmology [7] using various specially selected model systems in condensed matter, such as probing kinetics of cosmic string defects and the cosmological Kibble mechanism of their appearance using defects that occur at isotropic-nematic phase transition [8–14]. Recent advances in directly controlled generation, visualization, and manipulation of topological defects in condensed matter systems, such as liquid crystals (LCs) may provide a new means for experimental exploration of topological analogs to cosmic strings and Skyrmions and may probe topological aspects universal to these systems [15,16].

The ability to manipulate colloidal particles via noncontact optical techniques, such as laser tweezers, has enabled great advances in many scientific and technological fields [17–19]. Optical tweezers, including holographic optical tweezers (HOT), allow one to exert well-controlled forces (commonly within the range of 0.1–100 pN) and to reliably position and spatially translate individual particles or their arrays in three dimensions (3D) [17]. Although this enables noncontact manipulation of LC topological defects via the use of colloids as optically controllable "handles," there remain many limitations in this control strategy due to accessible optical force ranges, manipulatable degrees of freedom, and potential heating and realignment effects at the high laser powers needed to generate strong forces and torques [20]. Rotational manipulation is typically limited to rotations around the optical axis of the trapping beam and requires the use of Laguerre-Gaussian modes or the use of shape and/or optically anisotropic particles manipulated by laser beams with well-controlled polarization states. Finally, optical trapping is ineffective in media that are optically opaque to a trapping beam, such as LCs formed by high concentrations of graphene flakes and, in general, where the use of a highly focused trapping beam is impractical. Magnetic manipulation of colloids can supplement the inherent strengths of HOT and can mitigate some of the aforementioned limitations despite having its own weaknesses, mainly in terms of spatial translation and localization or selectivity. Magnetic fields can exert large torques on ferromagnetic or superparamagnetic colloids [21–23] in a highly controllable manner with minimal or no heating of the host material. Likewise, the LC host may be designed or selected and the magnetic field used within a limited range so that magnetic manipulation fields do not affect the LC director structure. Finally, magnetic manipulation is realizable in LC hosts that are optically opaque, highly birefringent, or

*Corresponding author: ivan.smalyukh@colorado.edu

otherwise possessing properties that render optical trapping impractical.

In this paper, we describe a robust method for magnetic and optical manipulations of topological defects using magnetic and optical colloidal handles (MOCH) in various LC hosts. This method allows us to manipulate the MOCHs and topological LC defects attached to them in a fully holonomic manner, i.e., in all three Cartesian degrees of freedom via HOT and in all three rotational degrees of freedom via magnetic control. Such combined magneto-optic manipulations allow us to probe the mechanical and structural properties of defects as well as to provide a powerful means for generating topologically and geometrically nontrivial defect configurations that would be difficult or impossible to achieve by optical or magnetic manipulation alone. We further supplement this magneto-optic manipulation technique by imaging with conventional polarizing optical microscopy (POM) and three-photon fluorescence excitation polarizing microscopy (3PEF-PM) applied in concert to simultaneously control and to probe topological line defects in nematic and cholesteric LCs.

II. MATERIALS, METHODS, AND TECHNIQUES

A. Integrated holonomic magnetic and holographic optical manipulation system

Our integrated holonomic magnetic and holographic optical manipulation system is shown in Fig. 1. Magnetic manipulation is achieved using three iron-core electromagnets (Fisher Scientific International, Inc. S52051 air-core solenoids with custom machined cast iron cores) arranged in a Cartesian frame machined from aluminum and mounted directly on the microscope body. The origin of the Cartesian frame is adjusted via shims. In some configurations, an ancillary Helmholtz coil is connected to a dc current source for high gradient magnetic-field pitch control, depth-resolved translation of defects, or to null magnetic-field gradients. A microscope slide holder is machined from aluminum and is positioned on the x-y plane using precision translation stages. Each electromagnet is independently driven via an amplified power supply (APS) BOP20-5M (obtained from Kepco). Each APS is voltage controlled using a computer-controlled data acquisition (DAQ) card (National Instruments USB-6259 BNC) and in-house LABVIEW-based software (LABVIEW was purchased from National Instruments). The electromagnets are ambient-air cooled with the aluminum harness acting as a heat sink, and therefore, continuous operation over several hours does not thermally affect our samples. Each electromagnet can produce ac (up to 8 Hz) and/or dc magnetic fields up to 40 Gs as measured at the sample by a Gauss meter. This field affects all magnetic particles in the sample volume and, thus, is appropriate for manipulation of multiple particles in a similar way simultaneously rather than manipulation of single colloids on an individual basis. The use of low magnetic fields assures robust control of magnetically responsive ferromagnetic and superparamagnetic particles without significant direct coupling between the magnetic field and the LC director. Since most known LCs (including the ones used in this study) are diamagnetic materials, director realignment is typically a thresholdlike effect and requires fields of 1000 Gs and higher at our studied cell thickness values, and therefore, the influence of up to 40 Gs magnetic fields (used in all magnetic manipulations presented herein) on the LC director **n** may be neglected in agreement with our experimental observations.

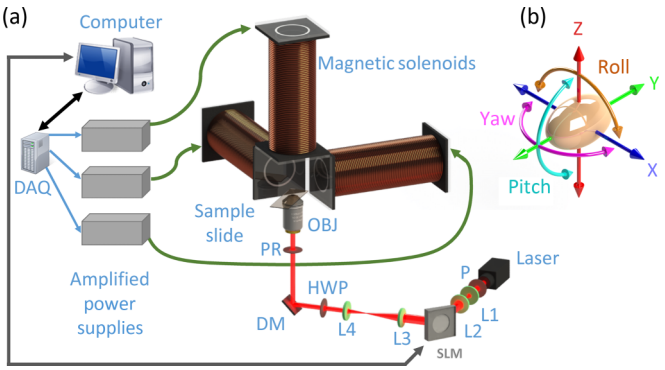

FIG. 1. (Color online) Integrated holonomic magnetic and holographic optical manipulation system. (a) Electromagnetic iron or air-core solenoids arranged in a Cartesian aluminum frame mounted on an inverted microscope (not shown). The solenoids are driven by amplified power supplies via computer-controlled DAQ. The HOT is based on a fiber laser and trapping system's optical elements: a polarizer (P), lenses (L1, L2, L3, and L4), a computer-controlled dynamically addressable liquid crystal based spatial light modulator (SLM), a 100 × oil immersion objective (OBJ), a half wave plate (HWP), a polarizer-rotator (PR), and a dichroic mirror (DM). The trapping beam is focused on the sample slide. (b) The magnetic and optical colloidal handles can be translated along the x, y, or z axes using the HOT and can be rotated in yaw, pitch, and roll using magnetic fields. This manipulation setup is integrated with an optical imaging system capable of both POM and 3PEF-PM imaging.

The magnetic colloids in our paper are superparamagnetic beads (SPMBs) (Dynabead M450, obtained from Invitrogen) with a nominal diameter of 4.5 ± 0.1 μm, which are fabricated using ferromagnetic nanoparticles (γFe_2O_3 and Fe_3O_4) approximately 8 nm in diameter and embedded into a highly cross-linked epoxy at a density of $\sim 10^5$ nanoparticles per bead. Although the nanoparticles are ferromagnetic, their small size allows thermally activated flipping of their magnetic moments [24] that can be characterized by the Néel relaxation time,

$$t = t_0 \exp\left(\frac{\kappa V}{k_B T}\right), \tag{1}$$

where t_0 is a material dependent preexponential attempt time on the order of 0.1–1 ns, k_B is Boltzmann's constant, T is the absolute temperature, and the product κV is the energy barrier for net magnetic moment flipping determined by the nanoparticles magnetic anisotropy energy density κ and volume V. Figure 2(a) shows a schematic of such a SPMB at no applied external field. The net magnetic moment of the SPMB is zero because its small volume sets the energy barrier product κV on the order of a few $k_B T$'s at room temperature. Random orientation of individual ferrite nanoparticles, coupled with this thermal moment flipping, creates a zero net magnetic moment in the SPMB. When an external magnetic field **H** is applied [Fig. 2(b)], the magnetic moment of a given ith ferrite nanoparticle ($\mathbf{m}_i$) is induced to favor one direction state along its easy axis, which may not necessarily align collinearly with **H**. It should be noted that, since the ferrite nanoparticle

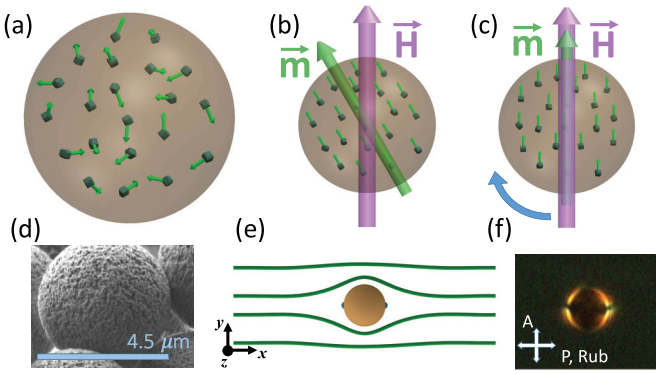

FIG. 2. (Color online) Superparamagnetic bead magnetic structure and surface anchoring. (a) A SPMB with a zero net magnetic moment is composed of ferrite nanoparticles fixed in an epoxy matrix. (b) An external magnetic field **H** is applied, inducing a transient net magnetic moment $\mathbf{m} = \Sigma \mathbf{m}_i$ at some angle with respect to **H**. (c) The generated magnetic torque aligns the beads magnetic moment **m** coaxially along **H**. Subsequent rotation of **H** rotates the SPMB. (d) SEM image of a SPMB showing surface roughness, indicating a strong surface anchoring which is tangential but with "memory" of director orientation at the surface. (e) The SPMB tends to distort the nematic director field, creating two surface point defects called "boojums," which are seen under polarizing optical microscopy (f). Orientations of polarizers and the rubbing direction are marked by white double arrows. Note that the boojum's coloring in (e) is a visual aid and is not meant to indicate charge or polarity.

orientations are mechanically coupled to the epoxy of the SPMB microsphere, the magnetic interactions with the applied field prompt transient SPMB rotation and alignment of the net induced magnetic moment **m** (due to the vector sum $\sum \mathbf{m}_i$) to eventually point along **H**. The ensuing torque on the epoxy matrix physically aligns the SPMB such that its net magnetic moment **m** locks to be collinear with **H** and is given by [22,25]

$$\mathbf{m} = V_p \chi_p \mathbf{H}, \tag{2}$$

where V_p is the colloid volume and χ_p is its effective magnetic susceptibility. Subsequent rotation of the magnetic field generates a torque on the SPMB as given by [21]

$$\boldsymbol{\tau} = \mu \mathbf{m} \times \mathbf{H}, \tag{3}$$

where μ is the colloid's magnetic permeability. The superposition of magnetic fields from each solenoid allows us to set **H** in any direction and to rotate this field at a given frequency, allowing us to achieve the desired rotation of the MOCHs. Since our experiment deals with low Reynolds number flow ($\mathrm{Re} \sim 10^{-7}$), we may neglect inertial effects and may roughly quantify the torque produced on our SPMB by balancing its rotational frequency with viscous drag in the LC host [26–28] as given by

$$\tau = \left(\frac{4\pi}{3}\right) \alpha R^3 \eta \Omega_c, \tag{4}$$

where R is the SPMB radius, η is the effective viscosity coefficient of the LC host, Ω_c is the critical decoupling frequency of the sphere rotation with respect to the external magnetic-field rotational frequency, and α is a numerical factor on the order of unity. We measured a magnetic torque of $\sim 5 \times 10^{-18}$ N m exerted on the particles in various LC systems.

In the presence of magnetic-field gradients, the force on a single colloid is proportional to the gradient of the magnetic field [29]. Although our manipulation system is designed to minimize this so-called "magnetic gradient force," the finite radius of the solenoid core results in a residual in-plane field gradient that can yield residual forces of up to 0.07 pN as estimated via balancing this magnetic force with a known viscous drag force. These residual gradient forces are found to be comparable to the gravitational force acting on these particles while dispersed in the LC and can, therefore, be neglected when particles are cotrapped by laser tweezers or localized within defects that typically have line tension on the order of tens of piconewtons.

In addition to interacting with field gradients, SPMBs can also interact magnetically with each other. For a collection of N colloids in an external field, the magnetic interaction force on a given colloid due to the other $(N-1)$ colloids in the presence of an applied external field is [30]

$$F_i = \frac{3\mu_0}{4\pi} \sum_{j=1, j\neq i}^{N} \frac{\hat{\mathbf{m}}_i \hat{\mathbf{m}}_j}{r_{ij}^4} \{[1 - 5(\hat{\mathbf{m}} \cdot \hat{\mathbf{r}}_{ij})^2]\hat{\mathbf{r}}_{ij} + 2(\hat{\mathbf{m}} \cdot \hat{\mathbf{r}}_{ij})\hat{\mathbf{m}}\}, \tag{5}$$

where $\mathbf{r}_{ij}$ is the distance between centers of the ith and jth colloids and $\hat{\mathbf{r}}_{ij}$ is the corresponding unit vector. However, no magnetic interactions are present when the field is turned off. By appropriately positioning (e.g., using laser tweezers) superparamagnetic particles within the sample, one can exert well-controlled interparticle forces that can be utilized in probing LC defects and structures. On the other hand, these forces can also be avoided by assuring that only single SPMBs or their clusters are present within the studied sample volume at distances within which these interaction forces are comparable to or stronger than thermal fluctuations.

Full holonomic control of a colloidal particle is achieved by combining mostly rotational magnetic manipulation with translational manipulation by HOT using a single integrated setup shown in Fig. 1 [31]. This allows us to define arbitrary positions and orientations of individual and multiple particles of interest. The HOT is built using a fiber laser operating at 1064 nm with output powers of up to 10 W (note that laser powers on the order of 1 mW per colloidal particle are typically sufficient for optical manipulation). The trapping beam passes through a polarizer (P) and two lenses (L1, L2) forming a telescope that is used to resize the beam diameter to slightly overfill the active area of a computer-controlled dynamically addressable LC-based spatial light modulator (SLM). The SLM generates a dynamic phase mask that creates and controls optical traps at a refresh rate of up to 20 Hz. After spatial modulation by the SLM, the trapping beam is linearly polarized in a desired orientation using a half wave plate and a polarizer and is subsequently directed via a second telescope (L3, L4) and reflection from a dichroic mirror to the back aperture of a 100 × oil immersion objective with a numerical aperture of NA = 1.42. Imaging is performed through a combination of POM and 3PEF-PM that are capable of operating in both epi-detection and forward-detection (transmission) modes with

the epi-detection mode being the primary configuration when implementing full three-axis holonomic manipulation.

B. Sample preparation

We use a commercial nematic mixture E-31 (from EM Chemicals) and a single-compound nematic LC pentylcyanobiphenyl (5CB, obtained from Frinton Laboratories). Cholesteric LC hosts are formed using one of these nematics doped with a small volume fraction of chiral agent (cholesteryl pelargonate obtained from Sigma-Aldrich Chemistry) to obtain chiral nematics with a cholesteric pitch in the range of 5–10 μm. In addition to the superparamagnetic beads discussed previously, we also use melamine resin spheres (obtained from Sigma-Aldrich Chemistry) 7 μm in diameter. All colloidal particles are dispersed in an LC host via either solvent exchange or sedimentation mixing with both methods yielding comparable dispersion efficiencies. Solvent exchange is performed by first vortex mixing the SPMB Dynabead carrier solution (de-ionized water with a density of 1×10^6 beads per μl) to disperse the beads evenly. Approximately 1 μl of this carrier is placed into a plastic vial and allowed to dry on a hot plate for 30 min after which 10 μl of isopropyl alcohol (IPA) is added and the mixture then sonicated at room temperature for 5 min to re-disperse the beads into the IPA. Some 100–200 μl of LC is subsequently added, and the mixture sonicated for an additional 10 min. The sample is placed in a water bath for 10 h at 95 °C to evaporate the solvent. Sedimentation mixing is accomplished by placing 1 μl of the Dynabead carrier on a well cleaned glass slide and evaporating on a hot plate at 100 °C for half an hour after which 1 to 2 μl of the LC host is added to the resulting sediment region on the slide, thoroughly mixed using a clean pipet tip, and dispersed into a larger volume of LC using vortex mixing for 30 s.

Cells are constructed from glass slide substrates cleaned in a water and detergent sonication bath at 60 °C, sequentially rinsed with acetone, methanol, and IPA, then dried, and plasma etched. Planar or homeotropic alignment of the cleaned substrates is set as determined by intended experiments. For planar anchoring, we spin coat the substrates with either polyvinyl alcohol (PVA 1% weight-to-weight ratio) in de-ionized water at 8500 rpm or with polyimide PI-2555 at 7500 rpm after which they are baked for at least 1 h at 100 °C. They are subsequently rubbed with a velvet cloth, which forces the LC molecules to align along the rubbing direction and, thus, sets planar boundary conditions for $\mathbf{n}(\mathbf{r})$. For homeotropic alignment, the cleaned substrates are immersed into dimethyloctadecyl[3-(trimethoxysilyl)propyl]ammonium chloride (DMAOP obtained from Arcos Organics) for 1 min and then allowed to dry in ambient air. The substrates are assembled in various configurations as needed for desired boundary conditions: planar cells with a director pretilt angle of ∼3°–6°, homeotropic cells, wedge cells, and twist cells. Cell thickness is typically set using spherical spacers dispersed in a UV curable epoxy (NOA-61, obtained from Norland Products) and varies from 10 to 120 μm, depending on the system under study. An LC host is infused into these cells via capillary forces and, subsequently, is sealed with fast setting epoxy.

The use of colloids as handles to manipulate director structures and defects depends greatly on the strength and nature of molecular interactions at the LC-colloid interface. POM studies [Fig. 2(f)] show that the particles induce tangential (planar) nondegenerate surface anchoring for $\mathbf{n}(\mathbf{r})$ of the LC where the director tends to pin to colloid surfaces, a phenomenon often referred to as the "anchoring memory effect." This behavior is consistent with the results of SEM imaging [Fig. 2(d)], which reveals nonuniform nanoscale surface morphology of a type that naturally allows for strong mechanical coupling between the superparamagnetic beads and various topological defects. Such coupling is an important aspect in our studies as discussed below.

III. RESULTS

A. Magnetic and holographic optical manipulation of cholesteric line defects using superparamagnetic beads

Noncontact manipulation of topological defects in LCs was previously accomplished either through polarized optical trapping of defect structures directly via refractive index contrast or through the use of colloids as "optical handles" to enhance polarization-independent optical trapping capabilities [32,33]. Our magnetic holonomic manipulation method employs superparamagnetic beads as "magnetic handles" and allows for robust, highly controllable three axis rotation of colloids around their own center of mass, enabling modes of control of defects that would be impossible via the use of HOT methods alone. Furthermore, our magneto-optical holonomic manipulation system inherits all the noncontact control capabilities of HOT with the only peculiarity that the superparamagnetic particles tend to absorb substantial amounts of trapping light, imposing limitations on the laser powers that can be used (typically limited to about 3 mW at the sample plane). On the other hand, this optical absorption is, in some ways, beneficial as it enhances available modes of defect manipulation by allowing us to induce local melting within the LC when high laser powers are used and, thus, enables optically induced highly localized nematic-isotropic phase transitions within the bulk of the sample.

We demonstrate the combined use of all of these noncontact control capabilities using examples of defect structures in various LC systems, starting with examples obtained for a cholesteric LC. Superparamagnetic particles are dispersed in a cholesteric LC (nematic host 5CB or E-31 doped with cholesteryl pelargonate at about 3.3 wt %) with pitch of about 5 μm as measured via direct 3PEF-PM imaging of sample cross sections. This dispersion is infused into planar cells with antiparallel rubbing and thicknesses between 30 and 60 μm. The samples are first studied with POM and 3PEF-PM to locate defects and to determine their type and structure. Holographic optical trapping allows localizing particles next to a defect, whereas, the SPMB-assisted local melting with laser light at higher powers of about 10 mW allows the particles to be "inserted" into a defect line with the ends of an "interrupted" linear defect being pinned to the diametrically opposite sides of the colloidal sphere.

Figure 3 shows magnetic and optical manipulations of a single dislocation of Burgers vector $|\mathbf{b}| = p/2$ with its core

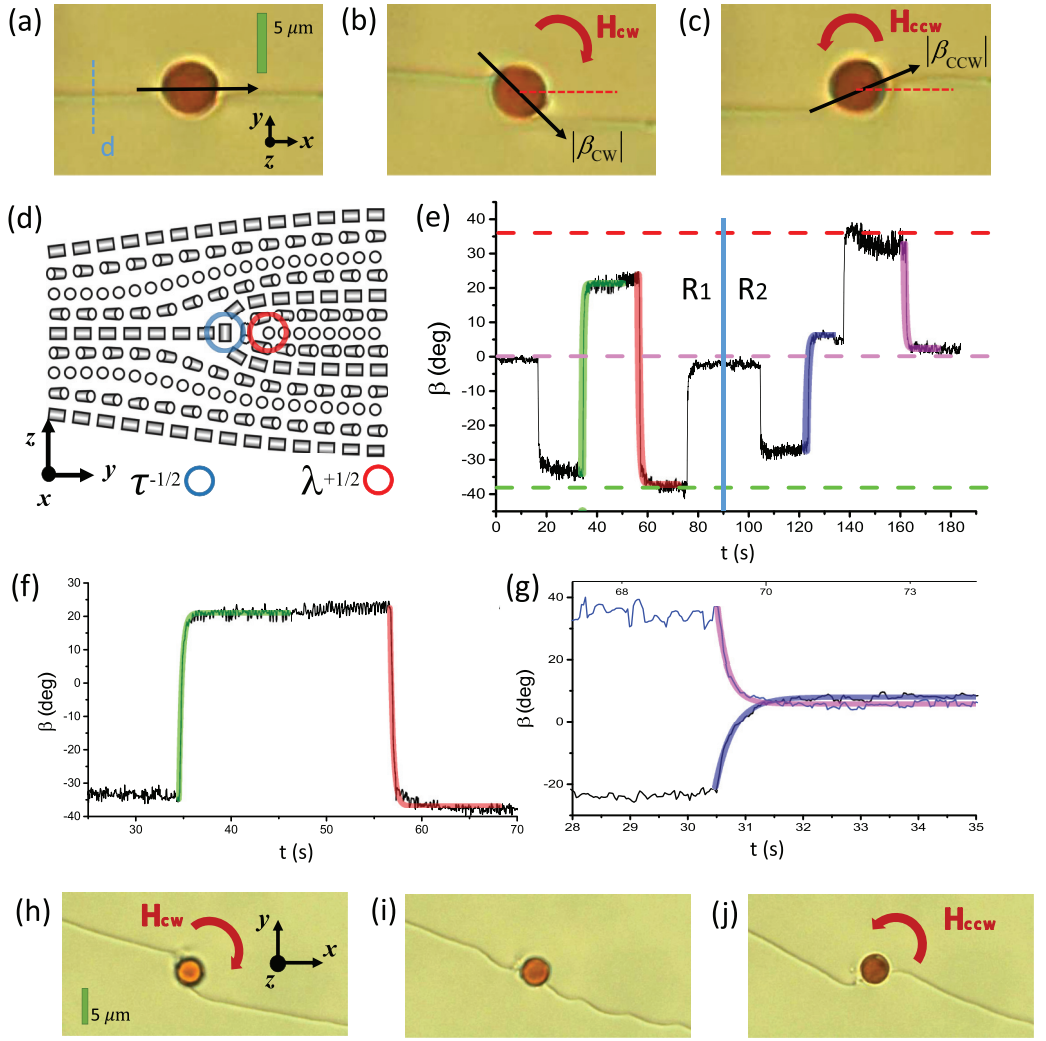

FIG. 3. (Color online) Manipulation of a dislocation defect line in a cholesteric liquid crystal by a single SPMB particle. (a) The SPMB is embedded into a cholesteric dislocation with a λ-τ defect core. The location of the cross-sectional plane corresponding to the structure of the dislocation core shown in (d) is marked by a blue (vertical) dashed line. (b) An ac magnetic field of ~40 Gs is rotated clockwise at a frequency of 8 Hz, which maximally rotates the SPMB to an angle β_{CW} and stretches the defect line. (c) At the same field amplitude and frequency, the SPMB is subsequently rotated counterclockwise to a maximum angle β_{CCW}. (d) Director structure of the manipulated topological defect with the λ-τ disclination core. (e) The defect structure's asymmetry seen from (d) causes a marked asymmetry in the defect's response to clockwise and counterclockwise bead rotation and in the difference between β_{CW} and β_{CCW}. Regions R_1 and R_2 denote the time periods during which the SPMB is forced between its maximum angles of rotation in two opposite directions via magnetic-field rotation (R_1) or is allowed to relax naturally (R_2). (f)–(g) Rotation angle (in degrees) vs time (in seconds) in the forcing regime and in the relaxing regime along with their exponential fit lines, respectively. (h)–(j) Optical POM micrographs showing a single dislocation with a λ-τ disclination pair which exhibits transient undulations along its length when manipulated in the forcing regime as discussed in the text.

composed of a λ-τ disclination pair in a 5CB-based cholesteric LC (CLC). At equilibrium, the particle is resting within the straight defect line, effectively interrupting it by introducing an isotropic spherical region into the singularity. The particle can also be localized in a region of strong elastic distortion near the core of the dislocation so that the two disclinations in the dislocation core remain uninterrupted. A colloid thus embedded into or pinned to a defect can be manipulated by translating it in different directions and, thus, moving the defect line, unless this translation is performed along the defect line, a direction in which the defect structure is translationally invariant. These types of manipulation are similar to what was achieved in the past by HOT alone [32]. However, when a controlled ac magnetic field of 40 Gs is applied and its direction rotated at a constant amplitude and a fixed frequency, we can achieve types of rotational manipulation of the colloidal handle and defect that cannot be realized using HOT alone. In the case of an interrupted dislocation with the defect-particle pinning at diametrically opposite sides of the colloidal sphere, which is most effective for this type of manipulation, the dislocation can be stretched during the rotation of the particle in clockwise (CW) or counterclockwise (CCW) directions via continuously rotating the magnetic field in a clockwise or counterclockwise direction, respectively [Figs. 3(b) and 3(c)]. By varying the frequency of the field rotation, we are able to maximally rotate the colloid and hold it near a fixed angle with a slight oscillation

about this angle due to the ac magnetic field temporarily losing phase lock with the SPMB rotation. Interestingly, this angle is different for clockwise and counterclockwise rotations and is, for example, approximately 25° and −40°, respectively, at a field rotation frequency of 8 Hz. This result is natural due to the apparent asymmetry of the director structure on the two opposite sides of the defect line [Fig. 3(d)].

By reversing the rotation of the field, the SPMB can be rotated to a new angle in a rapid manner, forcing the colloidal particle rotation from one maximum angle to another in the so-called "forcing regime" [Fig. 3(e), regime R_1]. Alternatively, by abruptly turning off the field, the colloidal particle is allowed to relax to its original orientation as the defect line straightens in order to minimize its corresponding free energy. This is the so-called "relaxation regime" R_2 [Fig. 3(e)]. The relaxation rotational motion is characterized by a balance of viscous and elastic torques where the elastic torque arises due to a combination of elastic distortions around the particle and defect line's tension. At small enough distortions from equilibrium, the colloid is expected to relax to its original orientation exponentially, $\beta(t) = \beta_0 e^{-t/\tau}$, where β_0 is the maximal SPMB rotation angle and τ is the relaxation time constant. Experimental colloidal particle rotation and relaxation data are shown in Fig. 3(e) along with exponential fits shown as differently colored lines. When forcefully rotating the SPMB between the maximal angles of −35° to 22° and back again [Fig. 3(f)], we obtain time constants of $\tau = 0.24$s [green (light-gray) line in R_1 left] and $\tau = 0.27$s [red (dark-gray) line in R_1 right], respectively. Video analysis of the SPMB in the relaxation regime [Fig. 3(g)] yields time constants of $\tau = 0.42$s [blue (gray) line in R_2 left] and $\tau = 0.34$s [magenta (medium-gray) line in R_2 right], respectively. This is again consistent with the effects of the defect's director field asymmetry on the embedded colloids rotational dynamics and the corresponding rotation of the twisted or stretched defect line, especially since the rotational motion of these particles in a cholesteric LC is coupled to its translation along the local orientation of the CLC helical axis.

An interesting effect occurs when a colloid is rapidly rotated from its maximal rotation angle to align again roughly along the defect line. Such manipulations induce undulations in the defect line due to the fact that the stretched disclination cannot contract fast enough (note that this contraction process is determined by the balance of elastic and viscous forces) to follow the fast rotation of the particle [Figs. 3(h)–3(j)]. The extra length of ∼10 μm results in transient undulations in the defect line with peaks arising and disappearing simultaneously in the course of about 1 s. Coupling the cholesteric helical structure to the angular rotation of the SPMB [20] also induces a translation in the vertical direction perpendicular to the cell substrates (which is also along the helical axis direction far from the defect), bending the dislocation out of the x-y plane upward or downward, depending on the direction of particle rotation with respect to the handedness of the LC. This effectively allows us to manipulate the dislocation with a λ-τ disclination core in different rotational and translational degrees of freedom.

Manipulation of defects provides an additional method for quantifying the torques that can be exerted by magnetically manipulated SPMBs. Since the defect line tension is known [27,32], we can estimate the torque applied to the line at the maximal deflection angle to be $\sim 2 \times 10^{-17}$ N m at an applied field of 40 Gs, comparable to that estimated using Eq. (4). SPMB chains allow for the application of even stronger torques, enabling considerable rapid distortions of defect lines as well as magnetic-field-assisted insertion and extraction of particles from defects. Figure 4 shows a pair of SPMB colloids manipulated by HOT while being colocated within a Lehmann cluster, which is achieved through localized melting of the LC surrounding the SPMBs. Relative motion of the SPMB pair within the defect can be controlled via a combination of dc magnetic dipole forces and linear confinement due to the defect core structure. As expected, aligning the applied dc magnetic field orthogonal to the defect line direction results in a repulsive dipole-dipole force that separates the SPMB pair, whereas, alignment with a field tangent to the defect line results in an attractive dipole-dipole force. It is possible to magnetically manipulate the pair in this manner as long as their surface-to-surface separation is larger than about 10% of the bead diameter, at which point, a colloidal dimer forms under the effect of defect- and medium-mediated attractive forces. Separation of the two particles from each other, subsequently, can be achieved by combining magnetic manipulation with local melting of the LC. Rotation of the SPMB pair is accomplished by use of an ac magnetic field in a manner similar to single particle rotation. As compared to the case of single SPMBs, such rotational manipulations yield larger maximal bend angles of defect lines at a given magnetic-field strength and frequency.

B. Full holonomic control of magnetic colloids to manipulate twist disclinations in nematic liquid crystals

Nematic LCs with mixed boundary conditions are known to host a wide variety of defects in transient, metastable, and stable configurations [34,35]. To demonstrate the power of our approach in noncontact manipulation of such defects, we introduce a nematic (5CB) MOCH particle dispersion into a twist/wedge cell formed by glass plates with rubbing directions aligned at 90° with respect to each other. The colloidal handles within the dispersion are composed of two species of particles, SPMBs and melamine resin microbeads. Due to the wedge geometry, the cell thickness ranges from 30 μm down to about 3 μm. To satisfy the strong surface boundary conditions at each confining glass plate, the director forms a twisted configuration across the sample thickness. Domains with ±90° twist across the cell thickness occur with about equal probability and are separated by defect lines, which we identify as twist disclinations (note that wall defects could be observed for submicron sample thicknesses but they are not observed in our experiments performed using our relatively thick twisted nematic cells [36]). In addition to occurring spontaneously upon quenching from an isotropic state, domains of opposite handedness and twist disclination loops can also be induced "on demand" by SPMB-assisted localized melting using in-sample laser powers of approximately 10 mW or higher with resulting disclinations of half-integer strengths [Fig. 5(a)]. Once the director structure is determined, circumnavigation of the defect line reveals that the LC director around defect cores

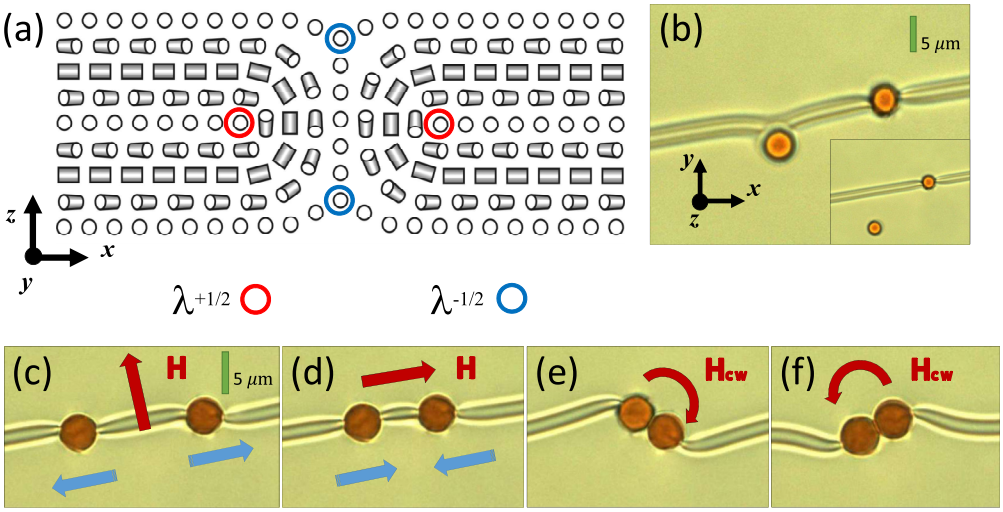

FIG. 4. (Color online) Magnetic and optical manipulation of two SPMB colloidal particles in a Lehmann cluster. (a) The director structure of the Lehmann cluster is composedof two $\lambda^{+1/2}$ and two $\lambda^{-1/2}$ topological defect lines [marked by red (left and right) and blue (top and bottom) open circles, respectively]. (b) Optical manipulation of two SPMBs as they are embedded into the Lehmann cluster. The inset shows an intermediate step of incorporation of the SPMB particles into the defect line. (c) and (d) Bright field optical micrographs reveal magnetic manipulation of relative positions of two SPMBs trapped within the Lehmann cluster defect line, which is achieved through magnetic dipole-dipole interactions while controlling the magnetic dipole orientations via changing the external field direction. Aligning the applied magnetic-field vector [dark (red) arrow] orthogonal to the defect line causes dipole-dipole repulsion [light (blue) arrows], whereas, aligning the magnetic-field vector parallel to the defect line leads to the dipole-dipole attraction. (e) and (f) Bright field optical micrographs depict magnetic torsion of a SPMB colloidal dimer while at two maximum particle-in-defect rotation angles; note that formation of a dimer allows for stronger magnetic torques and large rotation angles, providing modes of manipulation that cannot be achieved using a single SPMB.

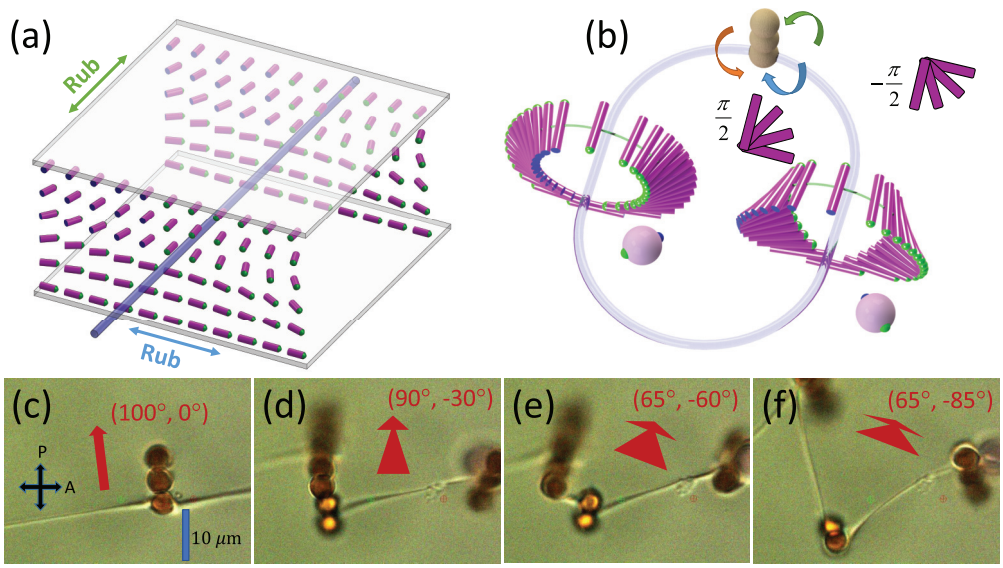

FIG. 5. (Color online) Full holonomic control of twist disclination loops in a $\pi/2$-twisted nematic cell. (a) Schematic of a twist disclination director structure and defect line (blue) in a $\pi/2$-twisted nematic cell; spatial variations in the director field are depicted using cylinders. (b) Schematic of the structure of the director field along the twist disclination loop; within a plane perpendicular to the twist disclination, the director circumscribes a Möbius strip. If the twist inside the loop is defined to be $+\pi/2$, or one quarter of a pitch, then the twist handedness outside the loop is $-\pi/2$. Colloids with tangential surface anchoring located in the cell midplane form surface point defects dubbed "boojums" that align at 45° to the two orthogonal rubbing directions set at the confining glass plates. Note that the molecule's and boojum's colorings in the schematics are visual aids and are not meant to indicate charge or polarity. Individual particles or particle chains, such as the trimer depicted in the schematic, can be colocated with the defect core. (c)–(f) An applied magnetic field of 40 Gs [with its in-plane and out-of -plane orientations indicated by red arrows and quantified by (θ, φ), where θ is the in-plane angle referenced from the x axis and φ is the azimuthal angle with respect to the x-y plane] is rotated in three dimensions, allowing for robust three-dimensional manipulation and stretching of the defect line.

twists by $\pm\pi$ while circumscribing the surface of a Möbius strip in a plane orthogonal to the disclination as shown in Fig. 5(b) with the interior cell region of the disclination loop possessing an oppositely handed twist to that of the exterior cell region. Optical manipulation at low laser powers (about 1 mW) allows us to embed MOCHs into these defects. Figures 5(c) and 5(d) show a twist disclination with several such embedded colloids forming chains. A magnetic field segregates or aggregates particles into various chain configurations and realigns them through a combination of defect line tension, magnetic torque, and dipole-dipole interparticle forces, thus, distorting the defect line in three dimensions. Varying the direction and magnitude of the applied magnetic field allows us to induce complex deformations of the defect line, such as the ones depicted in Figs. 5(e) and 5(f), which is enabled by the fact that different segments of the defect line are pinned to particles and colloidal chains that respond to holonomic magnetic and HOT optical control.

Twist disclinations are topologically stable nematic defects and cannot simply terminate in or interrupt in the bulk of a nematic LC, unless accompanied with melting of the sample or introducing isotropic inclusions. However, they do tend to form disclination loops of a net topological hedgehog charge equal to zero that can disappear via shrinking [36]. Figure 6 shows such a half-integer twist disclination loop. This shrinking process results in minimization of the overall free energy due to the elimination of additional elastic distortions and defects in-between the domains of opposite handedness and is the only process expected to take place, eventually leading to larger domains or a single domain of the same handedness of twist. Using our manipulation system, we demonstrate that such twist disclination loops can be split into multiple loops of smaller sizes, both having topological hedgehog charges equal to zero. A melamine resin bead mediates restructuring of the local director field near the defect line such that the original defect loop can be split into two smaller loops (Fig. 6). In this process, two segments of the initial defect loop are first attracted to and then attached to a colloidal particle's surface, consequently, locally merging and reconnecting into two smaller half-integer disclination loops. Both emerging loops of the twist disclinations have hedgehog charges equal to zero, and both are separating regions of opposite twist handedness with respect to their common exterior. Details of this reconnection are shown in experimental micrographs in Figs. 6(d)–6(g).

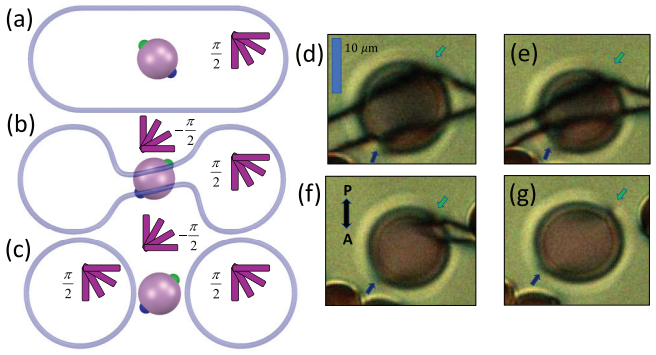

FIG. 6. (Color online) MOCH-mediated splitting of a twist disclination loop into two smaller loops. (a)–(c) Schematic showing reconnection or splitting progression of a twist disclination loop into two smaller disclination loops. The interior of the initial loop is defined with a twist of $+\pi/2$, whereas, the exterior is of twist $-\pi/2$. A melamine resin bead with planar surface anchoring induces two boojum defects that localize at the poles along the local director of the twisted structure in the cell midplane. During reconnection and defect loop splitting, the MOCH rotates by $\pi/2$ as can be seen by comparing parts (a) and (c). (d)–(g) Optical micrographs showing the time progression of a twist disclination loop splitting into two smaller loops, whereas, these defects are sliding on the surface of a 7 μm diameter melamine resin bead, eventually leading to two smaller defect loops, both being separated from the bead. Note the orientation of the boojums (indicated by small arrows) during reconnection. The double arrow in (f) marks orientations of the polarizer and analyzer, which were aligned parallel to each other.

C. Patterning of cholesteric fingers in a frustrated cholesteric system

Cholesteric LCs confined in homeotropic cells are known to exhibit localized solitonic structures and defects, such as cholesteric fingers, torons, and other configurations that appear due to incompatibility of vertical surface boundary conditions and a uniform helicoidal structure. These solitonic structures can arise either spontaneously or when generated by electric fields or focused laser beams [34,35]. In this section, we show that holonomic magnetic manipulation of colloids allows us to explore different aspects of this system that cannot be probed by other noncontact manipulation techniques.

SPMB colloids are dispersed into a CLC based on an AMLC-001 (from AlphaMicron, Inc.) nematic host and chiral additive CB-15 (from EM Chemicals) added at a percentage needed to yield an equilibrium pitch of $p = 9$ μm. This dispersion is then infused into a wedge cell with homeotropic boundary conditions and thicknesses ranging from $d = 7$ to 10 μm. Cholesteric fingers (Fig. 7) form in regions where the confinement parameter $c = d/p = 0.75$–1.0. There are at least four classes of cholesteric fingers [34,35], the most common being the species of the first and second kinds denoted as CF-1 and CF-2, respectively. Figures 7(a)–7(f) show CF-1s with SPMB dimers and trimers located in the defects and in the CLC bulk. An initial in-plane clockwise rotation of a 40 Gs magnetic field at 0.25 Hz produces a clockwise rotational motion of the dimers, which winds two CF-1s into spiral configurations [Fig. 7(a)]. It should be noted that, although CF-2 fingers were previously observed spontaneously forming spirals in an applied ac electric field, which was attributed to the inherent asymmetry in their structure [34,35], CF-1 fingers are not known to form spirals spontaneously or in response to applied fields. This can be understood by considering the symmetry of their translationally invariant director structure with a cross section shown in Fig. 7(g). It is, therefore, interesting that, without spatial translation, magnetically rotated SPMBs, which are mechanically coupled to the finger's structure via elastic distortion sharing, can promote the formation of spiral configurations in CF-1 fingers. By subsequently reversing the magnetic-field rotation, we can partly reverse this winding, eventually forming a spiral

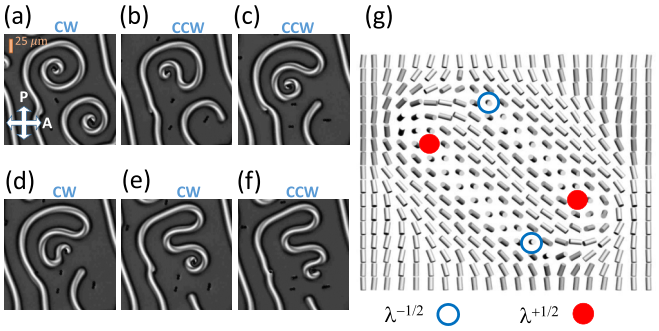

FIG. 7. (Color online) Manipulation of cholesteric fingers in a cholesteric LC cell with homeotropic boundary conditions. (a) Two CF-1 fingers are manipulated using two different SPMB dimers that are rotated via magnetic-field rotation. (b) Reversing rotation partly unwinds one of the two CF-1s, whereas, the SPMB dimer "escapes" from the second CF-1 finger. (c) A meanderlike configuration is formed from one of the two CF-1s, whereas, the other CF-1 relaxes to its natural linear state. (d)–(f) Repeated reversal of magnetic-field rotation allows us to create an arbitrary number of CF-1 meanders and spirals. (g) Director structure of the CF-1 finger composed of two $\lambda^{-1/2}$ and $\lambda^{+1/2}$ disclinations [marked by open (blue) and red (closed) circles, respectively].

of opposite handedness [Fig. 7(c)]. Figures 7(b)–7(f) also show that the elastic attachment of the SPMB to the finger is important for this manipulation because the bottom finger spiral, which detached from its dimer, has relaxed to its expected straight finger line configuration as the sequence progresses. By repeated reversals of the magnetic rotation, one can "draw" CF-1 meanders and spirals of significant complexity. One should mention here that the spiraling and meanderlike structures of the fingers shown here are still transient or metastable configurations that can eventually relax to straight finger lines. Although similar configurations of cholesteric fingers could be optically patterned by scanned laser beams as we have demonstrated previously [37], it is interesting that our magnetic manipulation method allows for accessing them through rotational manipulation alone.

D. Kink chain generation in Lehmann clusters

In the past, laser manipulation studies of defects, including disclinations, oily streaks, edge dislocations, and Lehmann clusters, have allowed exploration of defect properties, such as line tension and topological stability [33]. An interesting new manipulation capability enabled by our magnetic holonomic control of colloidal handles involves rotational torsion of defect lines as demonstrated above using several examples of defects in nematic and cholesteric LCs. This capability also allows us to produce so-called "kinks" [32] in topologically unstable Lehmann clusters of disclination defects that appear in layered cholesteric structures (Fig. 8). Lehmann clusters are composed of quadrupoles of nonsingular half-integer λ disclinations of opposite signs and, thus, have a net winding number (strength) equal to zero. In terms of the cholesteric layered structure, these defects separate sample regions with the same number of cholesteric layers and, therefore, have a net Burgers vector also equal to zero. This makes them very different from topologically stable defect lines, such as the twist disclinations and edge dislocations discussed in previous sections because these defect clusters can terminate on the SPMB particles that we use for manipulation. Our combined magnetic and optical manipulations allow for controlled generation of Lehmann clusters via the optical translation of particles and the generation of various kinks within them via particle rotation. Figure 8 details how we generate multiple kinks in a Lehmann cluster via magnetic manipulation of SPMB colloids attached to its end. We can adjust the number of kinks by selectively unwinding the Lehmann cluster or by generating antikinks with opposite winding of the defect cluster, which typically is followed by pair annihilation of the kink or antikink pair. The strong pinning of the Lehmann cluster's end to a given particle [with the nanostructured surface morphology shown in Fig. 2(d)] is essential to our manipulation process.

Figure 9 details an example of kink generation in a Lehmann cluster using SPMBs that are magnetically rotated clockwise. To preserve the nonsingular nature of the λ disclinations within the cluster, this rotation locally translates the cluster in the vertical negative z direction while also lengthening and bending the cluster in the x-y plane. Continued rotation eventually pulls the colloid along z by one cholesteric pitch at which point the cluster is turned through 360° so that the kink is fully formed in the Lehmann cluster defect line. The resulting kink adopts the curvature of distortion of the Lehmann cluster and is approximately equal to one cholesteric pitch in diameter. By reversing the colloid rotation, we can either unwind the kink by reversing the generation stages depicted in Fig. 9 or, in some cases, generate an antikink of opposite winding that eventually annihilates with the initial kink [Fig. 8(e)]. Interestingly, in cases when magnetic manipulation alone is used to generate a series of kinks, line tension tends to minimize the defect line length and, thus, limits the number of kinks that can be generated as this number is constrained by the number of layers in the cholesteric structure that the defect is crossing. By supplementing this magnetic noncontact control with linear optical manipulation and pinning of defects to particles and cell surfaces, we are able to rotate, stretch, and translate a defect line holonomically, allowing complex manipulations that may allow one to explore interesting topological configurations, potentially including free-standing knots and different types of linked defect loops.

IV. DISCUSSION

Our current study focused on examples of linear and rotational defect manipulations in nematic and cholesteric LCs, e.g., in mesomorphic phases with only orientational ordering. However, these studies can be extended to nematic point and wall defects in such mesophases as well as to a variety of different types of defects in LC phases with various degrees of partial long-range or quasi-long-range positional ordering. Defect structures that can be effectively probed by magnetic and optical holonomic controls may include focal domains in smectics, developable domains in columnar phases, and dispirations in smectics with antiferroelectric ordering. Although rotation of dielectric microspheres in smectic LCs was previously accomplished by applying dc or low-frequency ac fields

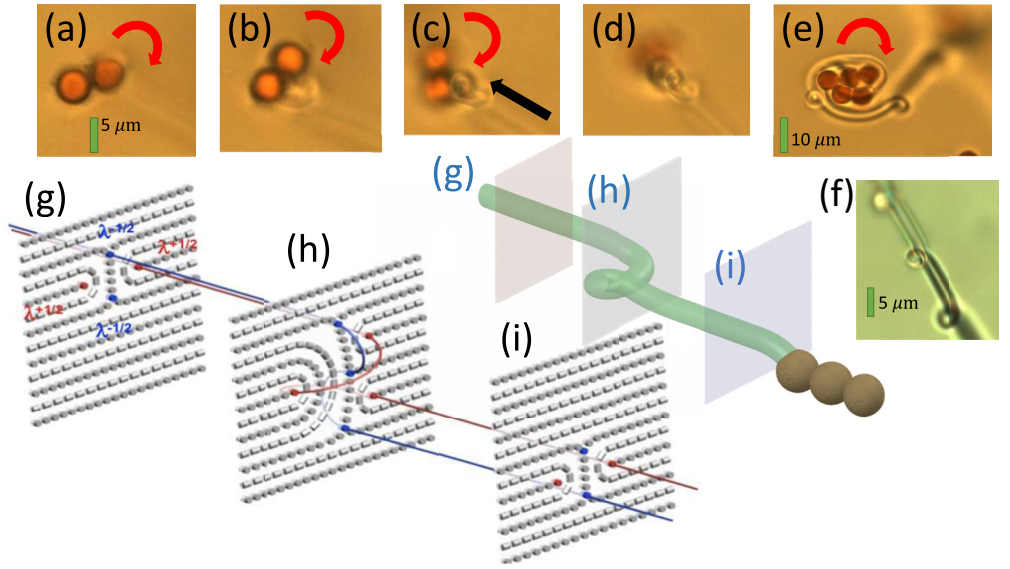

FIG. 8. (Color online) Generation of a series of kinks in a cholesteric Lehmann cluster. (a) A SPMB colloidal dimer is attached to a Lehmann cluster defect and is magnetically rotated clockwise [as shown by a red (curved) arrow] in the x-y plane. (b)–(d) Several kinks (marked by a black arrow) are generated by continuous rotation of the SPMBs. Note the defocusing of the SPMBs indicates a translation of the defect along the vertical z-direction axis. (e) A kink and antikink pair generated by magnetic rotation in another Lehmann cluster attached to a colloidal aggregate. The antikink is seen closer to the aggregate and was generated by reversing the rotation direction as compared to that used to generate the kink in the same defect line. With time, the antikink eventually annihilates with the kink. (f) A well-defined series of equidistant kinks is formed in a Lehmann cluster due to repulsive interactions between the generated kinks. (g)–(i) Schematics of the director field in different cross-sectional planes, which represent the evolution of the director structure along the Lehmann cluster defect line with a kink. (g) A Lehmann cluster is shown with representative blue and red lines (light gray and dark gray lines, respectively) corresponding to $\lambda^{-1/2}$ and $\lambda^{+1/2}$, respectively. (h) Cross section of the kink tracing the path of the $\lambda^{-1/2}$ and $\lambda^{+1/2}$ defects. (i) The Lehmann cluster's position across the cholesteric layers has been shifted in the vertical z direction (along the direction of the cholesteric helix axis far from the defect).

[37], the particles could only be rotated around certain well defined axes predetermined by the geometries of electrodes and samples (unlike in our case of unrestricted holonomic rotational control), and its possible use in the manipulation of defects has not been explored. The holonomic control of colloidal particles in various smectic and columnar phases may yield the means of generating new defect structures as well as controlling preexisting defects. Whereas, magnetic fields for particle manipulation in nematic and cholesteric phases need to be kept below 50 Gs to avoid significant effects of diamagnetic coupling directly to the LC director in these highly responsive mesophases, higher fields of up to ~500 Gs can be applied to manipulate particles in phases with partial positional ordering because magnetic realignment effects in these systems are typically hindered by the presence of this positional ordering. Although our study specifically avoided the use of strong magnetic-field gradients for spatial localization and translation of colloids, such capabilities can be added. Additional advantages and new possibilities in this case would arise from stronger particle localization induced by high magnetic-field gradients and the application of far stronger linear forces as compared to what can be achieved using optical tweezers. In addition to samples confined between parallel glass plates, manipulation of defects can also be performed in other confinement geometries, such as droplet geometries and free-standing films as well as in various mesomorphic phases with defects in the ground state (such as blue phases and twist grain boundary phases) in which studies of defects by laser tweezers are typically limited due to the fact that the use of immersion-oil high-numerical-aperture objectives is impractical.

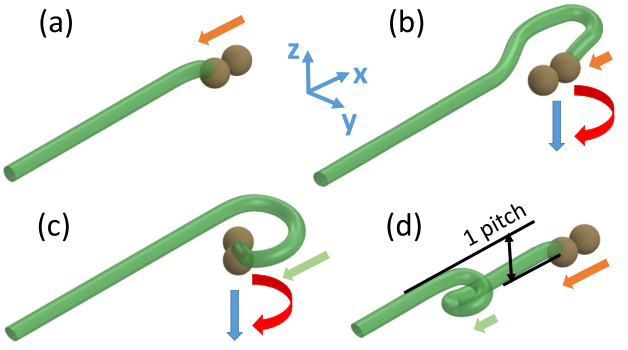

FIG. 9. (Color online) A schematic of generating kinks in a Lehmann cluster using magnetically controlled beads. (a) A colloidal dimer attached to a Lehmann cluster's end is translating linearly due to minimizing line energy as shown by the orange (light gray) arrow. (b) As the dimer is rotated clockwise by 180° [dark (red) arrow], it moves along the vertical z axis by $\frac{1}{2}$ pitch [gray (blue) arrow], which is due to the need of preserving the low-energy nonsingular nature of the Lehmann cluster's defect core and due to the coupling of rotation to translation along the helical axis of cholesteric LCs [30]. (c) and (d) Continuous colloidal dimer rotation generates a kink in the Lehmann cluster, which shifts the axial position of this defect in the cholesteric layered structure. The far-field helical axis of the CLC is aligned along the vertical z direction.

By combining three-dimensional spatial translation of MOCHs mechanically coupled to defects with torsion of

defects induced by their rotation and with various types of laser-induced local melting of the LC, one may be able to control twist and writhe [38–40] of defect lines forming loops, and thus, one may be able to generate defect loops with nonzero topological hedgehog charges. This potentially can be performed for individual or multiple defect loops that may or may not be linked with each other. Another interesting direction of extending the present work may involve generation of topologically nontrivial configurations of defect lines in the forms of various free-standing knots, links, etc. Although our manipulation method is geometrically unrestricted in terms of the defect manipulation, such restrictions will be self-imposed naturally by topological constraints inherent in various LC systems, which, therefore, may allow one to explore the interplay of topologies of nematic director fields, defects, various loops, surfaces, etc. With careful calibration of magnetic forces and torques exerted on SPMBs, MOCHs may also allow for experimental exploration of mechanical properties of defect lines and wall defects, which remain poorly understood. By using nanoparticles instead of relatively large SPMB microbeads, one can potentially probe the core structure of defects and can explore variations in rheological properties within LC samples containing defects, etc.

V. CONCLUSION

We have developed an integrated magnetic and optical manipulation system for full holonomic control of topological defect lines in nematic and cholesteric liquid crystals. The rotational manipulation of colloidal chains and pinning of defects to colloidal particles allows us to form complex 3D patterns of defects not found naturally in liquid crystal systems, such as spirals in cholesteric fingers of the first kind. Furthermore, we have been able to integrate this magnetic rotational manipulation with linear holographic optical trapping in such a way as to enhance the strengths of each while ameliorating the inherent weaknesses in either method alone. Using specific examples, we demonstrated that our method provides powerful new tools for the study of topological defects as well as potentially allowing one to create fascinating topological defect configurations, such as free-standing knots and links of defects. Such exploration may be of interest not only from the standpoint of a general understanding of defects in condensed matter, but also for their use in modeling topological defects in early universe cosmology, string theory, high energy physics, and other physical systems.

ACKNOWLEGMENTS

We acknowledge discussions with J. Evans, B. Senyuk, M. Pandey, P. Ackerman, T. Lee, C. Twombly, B. Schwab, and R. L. Clark. We especially thank Q. Zhang for his assistance with sample and cell preparation and AlphaMicron, Inc. for providing AMLC-001. This work was supported, in part, by NSF Grant No. DMR-0847782 (M.C.M.V. and I.I.S.).

[1] A. Vilenkin and E. P. S. Shellard, *Cosmic Strings and Other Topological Defects* (Cambridge University Press, Cambridge, UK, 1994).
[2] *Phase Transitions in the Early Universe: Theory and Observations*, edited by H. J. D. Vega, I. M. Khalatnikov, and N. G. Sànchez, NATO Science Series II: Mathematics, Physics and Chemistry, Vol. 40 (Springer, Dordrecht, 2001).
[3] M. R. DePies and C. J. Hogan, Phys. Rev. D **75**, 125006 (2007).
[4] D. Bailin and A. Love, *Cosmology in Gauge Field Theory and String Theory* (Institute of Physics, Bristol, 2004).
[5] I. Chuang, B. Yurke, A. N. Pargellis, and N. Turok, Phys. Rev. E **47**, 3343 (1993).
[6] P. A. R. Ade *et al*. (Planck Collaboration), arXiv:1303.5085.
[7] J. C. Long, H. W. Chan, A. B. Churnside, E. A. Gulbis, M. C. Varney, and J. C. Price, Nature (London) **421**, 922 (2003).
[8] T. W. B. Kibble, J. Phys. A **9**, 1387 (1976).
[9] W. H. Zurek, Nature (London) **317**, 505 (1985).
[10] S. N. Fisher, A. M. Guénault, C. J. Kennedy, and G. R. Pickett, Phys. Rev. Lett. **69**, 1073 (1992).
[11] P. C. Hendry, N. S. Lawson, R. A. M. Lee, P. V. E. McClintock, and C. D. H. Williams, Nature (London) **368**, 315 (1994).
[12] D. I. Bradley, Y. M. Bunkov, D. J. Cousins, M. P. Enrico, S. N. Fisher, M. R. Follows, A. M. Guénault, W. M. Hayes, G. R. Pickett, and T. Sloan, Phys. Rev. Lett. **75**, 1887 (1995).
[13] M. J. Bowick, L. Chandar, E. A. Schiff, and A. M. Srivastava, Science **263**, 943 (1994).
[14] I. Chuang, R. Durrer, N. Turok, and B. Yurke, Science **251**, 1336 (1991).
[15] J. S. Evans, P. J. Ackerman, D. J. Broer, J. van de Lagemaat, and I. I. Smalyukh, Phys. Rev. E **87**, 032503 (2013).
[16] P. J. Ackerman, Z. Qi, and I. I. Smalyukh, Phys. Rev. E **86**, 021703 (2012).
[17] D. B. Conkey, R. P. Trivedi, S. R. Pavani, I. I. Smalyukh, and R. Piestun, Opt. Express **19**, 3835 (2011).
[18] G. Cipparrone, A. Mazzulla, A. Pane, R. J. Hernandez, and R. Bartolino, Adv. Mater. **23**, 5773 (2011).
[19] M. R. Dennis, R. P. King, B. Jack, K. O'Holleran, and M. J. Padgett, Nat. Phys. **6**, 118 (2010).
[20] D. Engström, M. C. Varney, M. Persson, R. P. Trivedi, K. A. Bertness, M. Goksor, and I. I. Smalyukh, Opt. Express **20**, 7741 (2012).
[21] R. M. Erb, N. J. Jenness, R. L. Clark, and B. B. Yellen, Adv. Mater. **21**, 4825 (2009).
[22] Y. Gao, M. A. Hulsen, T. G. Kang, and J. M. J. den Toonder, Phys. Rev. E **86**, 041503 (2012).
[23] Z. G. Forbes, B. B. Yellen, K. A. Barbee, and G. Friedman, IEEE Trans. Magn. **39**, 3372 (2003).
[24] Q. A. Pankhurst, J. Connolly, S. K. Jones, and J. Dobson, J. Phys. D **36**, R167 (2003).
[25] R. J. S. Derks, A. Dietzel, R. Wimberger-Friedl, and M. W. J. Prins, Microfluid. Nanofluid. **3**, 141 (2007).
[26] I. Sinn, T. Albertson, P. Kinnunen, D. N. Breslauer, B. H. McNaughton, M. A. Burns, and R. Kopelman, Anal. Chem. **84**, 5250 (2012).
[27] Q. Liu, T. Asavei, T. Lee, H. Rubinsztein-Dunlop, S. He, and I. I. Smalyukh, Opt. Express **19**, 25134 (2011).

[28] S. S. Shevkoplyas, A. C. Siegel, R. M. Westervelt, M. G. Prentiss, and G. M. Whitesides, Lab. Chip **7**, 1294 (2007).
[29] J. D. Jackson, in *Classical Electrodynamics* (Wiley, New York, 1999), p. 808.
[30] S. Melle, O. G. Calderón, M. A. Rubio, and G. G. Fuller, Phys. Rev. E **68**, 041503 (2003).
[31] R. P. Trivedi, T. Lee, K. A. Bertness, and I. I. Smalyukh, Opt. Express **18**, 27658 (2010).
[32] R. P. Trivedi, D. Engström, and I. I. Smalyukh, J. Opt. **13**, 044001 (2011).
[33] R. P. Trivedi, I. I. Klevets, B. Senyuk, T. Lee, and I. I. Smalyukh, Proc. Natl. Acad. Sci. USA **109**, 4744 (2012).
[34] P. Oswald, J. Baudry, and S. Pirkl, Phys. Rep. **337**, 67 (2000).
[35] J. Baudry, S. Pirkl, and P. Oswald, Phys. Rev. E **59**, 5562 (1999).
[36] S. Chandrasekhar, in *Liquid Crystals* (Cambridge University Press, Cambridge UK/New York, 1993), p. 460.
[37] I. I. Smalyukh, B. I. Senyuk, P. Palffy-Muhoray, O. D. Lavrentovich, H. Huang, E. C. Gartland, Jr., V. H. Bodnar, T. Kosa, and B. Taheri, Phys. Rev. E **72**, 061707 (2005).
[38] G. Liao, I. I. Smalyukh, J. R. Kelly, O. D. Lavrentovich, and A. Jákli, Phys. Rev. E **72**, 031704 (2005).
[39] S. Čopar and S. Žumer, Phys. Rev. Lett. **106**, 177801 (2011).
[40] U. Tkalec, M. Ravnik, S. Čopar, S. Žumer, and I. Muševič, Science **333**, 62 (2011).